

# Seismic Evaluation of Hazard-Resistant Pipelines: PVC, PVCO, and iPVC Pipe with Coupling

## Axial Testing Report

Submitted to:

Timothy Harris & David Katzev  
East Bay Municipal Utility District

Prepared by:

C. R. Ihnotic  
J. L. Ramos  
B. P. Wham



Center for Infrastructure, Energy, and Space Testing  
Civil, Environmental, and Architectural Engineering  
University of Colorado Boulder  
Boulder, CO 80309

December 2019



## Table of Contents

Table of Contents .....	ii
List of Figures .....	iii
List of Tables .....	iv
1. Introduction .....	1
1.1. Test Specimens .....	1
1.2. Test Overview .....	2
2. General Test Setup and Protocols .....	3
2.1. Axial Test Setup .....	3
2.1.1. Specimen Installation Procedure .....	3
2.1.2. Instrumentation .....	6
2.2. Test Procedure .....	7
2.2.1. Pretest .....	7
2.2.2. Test Sequence .....	8
2.2.3. Stop or Pause Criteria .....	8
3. Axial Tension Results .....	9
3.1. Tension Test PT01 Results .....	9
3.2. Tension Test PT02 Results .....	11
3.3. Tension Test PT05 Results .....	14
3.4. Tension Test PT09 Results .....	16
3.5. Comparison of Tension Test Results .....	19
4. Axial Compression Test .....	21
4.1. Compression Test PC06 Results .....	21
5. Axial Cyclic Tests .....	26
5.1. Cyclic Test PS12 Results .....	26
5.2. Cyclic Test Comparison .....	29
6. Summary and Conclusions .....	31
Acknowledgements .....	33
References .....	33
Appendix A Pressurization Sequence .....	34



## List of Figures

Figure 1.1. Examples of the RCT Flex-Tite (a) coupling and (b) tee .....	2
Figure 2.1. Pipe specimen in axial test frame .....	3
Figure 2.2. Dimensioned drawing of axial test setup.....	4
Figure 2.3. Marked measurements on non-cut ends of the pipe. ....	4
Figure 2.4. Identifying the pipe coordinates (crown, invert, springlines).....	4
Figure 2.5. Pipe connections to loading frame.....	5
Figure 2.6. Megalug restraints on “cut” ends of pipe .....	5
Figure 2.7. Fixed end (east) with water intake and pressure valve .....	5
Figure 2.8. Specimen instrumentation .....	7
Figure 3.1. Specimen PT01 (a) before and (b) after axial tension test.....	9
Figure 3.2. PT01 results for internal pressure, actuator displacement and axial force vs. time.....	10
Figure 3.3. Specimen PT01 actuator force vs. (a) measured axial displacements and (b) total joint displacement at north and south springline string pots .....	10
Figure 3.4. Specimen PT01 after failure: (a) circumferential fracture and (b) test overview .....	11
Figure 3.5. Specimen PT02 (a) before and (b) after axial tension test.....	12
Figure 3.6. PT02 pressure, axial load, and actuator displacement vs. time .....	12
Figure 3.7. PT02 Axial Force vs Actuator Displacement .....	13
Figure 3.8. PT02 Force vs Joint Displacement .....	13
Figure 3.9. PT02 axial and circumferential strains .....	13
Figure 3.10. Specimen PT05 results for pressure, axial force, and actuator displacement vs. time .....	14
Figure 3.11. PT05 Force vs Actuator Displacement.....	15
Figure 3.12. PT05 Force vs Joint Displacements.....	15
Figure 3.13. LVDTs (top) and string potentiometer (bottom) locations for PT05.....	15
Figure 3.14. Failure at east joint for PT05 .....	15
Figure 3.15. PT05 Average axial and circumferential strains vs. (a) time and (b) axial force .....	16
Figure 3.16. Specimen PT09 results for pressure, axial force, and actuator displacement vs. time .....	16
Figure 3.17. PT09 Force vs Actuator Displacement.....	17
Figure 3.18. PT09 Force vs Joint Displacements.....	17
Figure 3.19. LVDT locations for PT09.....	18
Figure 3.20. Failure at west joint for PT09 .....	18
Figure 3.21. PT09 Average axial and circumferential strains vs. time and axial force .....	18



Figure 3.22. Tension Test Comparison for Axial Force vs Act. Disp..... 20

Figure 3.23. Tension Test Comparison for Axial Force vs Joint Disp..... 20

Figure 3.24. Tension Test Comparison for Axial Force vs Axial Strain. .... 20

Figure 3.25. Tension Test Comparison for Axial Force vs Circ. Strain. .... 20

Figure 4.1. Compression test setup ..... 21

Figure 4.2. Megalug end restrain orientation for compression ..... 21

Figure 4.3. Specimen PC06 results for pressure, axial force, and actuator displacement vs. time ..... 22

Figure 4.4. PC06 Force vs Actuator Displacement..... 23

Figure 4.5. PC06 Force vs Joint Displacements ..... 23

Figure 4.6. LVDT and String Potentiometer locations for PC06..... 23

Figure 4.7. Buckle at east joint for PC06..... 23

Figure 4.8. PC06 axial strain (a) and circumferential strain (b) vs. time ..... 24

Figure 4.9. Images of PC06 loading progression..... 25

Figure 5.1. Megalug end restrain orientation for cyclic loading..... 26

Figure 5.2. Specimen PS12 results for pressure, axial force, and actuator displacement vs. time ..... 27

Figure 5.3. PS12 force vs actuator displacement ..... 27

Figure 5.4. PS12 force vs axial displacements..... 28

Figure 5.5. LVDT locations for PS12..... 28

Figure 5.6. Failure at joint for PS12..... 28

Figure 5.7. PC06 axial strain (a) and circumferential strain (b) vs. time ..... 29

Figure 5.8. Tension Test Comparison for Axial Force vs Act. Disp. .... 30

Figure 5.9. Tension Test Comparison for Axial Force vs Joint Disp. .... 30

Figure 5.10. Tension Test Comparison for Axial Force vs Axial Strain. .... 30

Figure 5.11. Tension Test Comparison for Axial Force vs Circ. Strain. .... 30

Figure 6.1. PS12 pressurization sequence, pressure vs time..... 34

Figure 6.2. Circumferential (a) and Axial (b) strain vs time..... 35

**List of Tables**

Table 1.1. Summary of Tests and Specimens ..... 2

Table 3.1. Summary of Axial Tension Test Results ..... 19

Table 6.1. Summary of Test Results ..... 31



## 1. Introduction

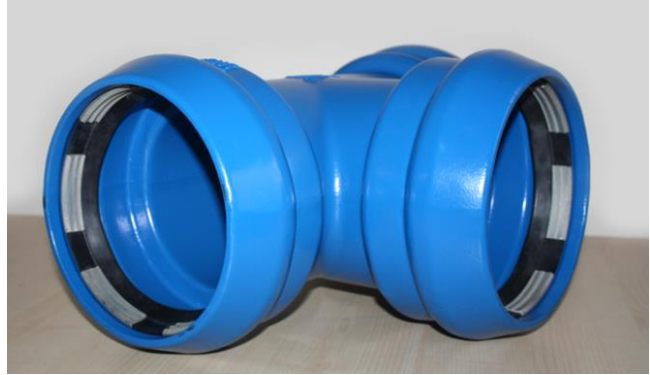
This report is submitted to the East Bay Municipal Utility District (herein referred to as EBMUD). It presents test results from a program to investigate the axial performance of nominal 6 in. (150 mm) diameter thermoplastic pipe with couplings. The work was undertaken in the Center for Infrastructure, Energy, and Space Testing which is affiliated with the Civil, Architectural, and Environmental Engineering Department at the University of Colorado Boulder.

The intention of this study is to impose external loading conditions to the test specimens that are representative of the significant deformations possible during earthquake-induced ground deformation such as landsliding, fault rupture, and liquefaction-induced lateral spreading, thus characterizing the pipeline system capacity. Specimens are internally pressurized to mimic in-situ conditions to best understand how these systems will behave in the field. As detailed, all tests were designed and performed in accordance with procedures and recommendations provided by Wham et al. (2018).

The report is organized into six sections. Section 1 provides introductory remarks, including discussion of the test specimens and experimental overview. Section 2 presents the general axial test setup and experimental protocols. Section 3, 4 and 5 discuss axial tension, axial compression, and axial cyclic tests, respectively. Finally, Section 6 provides a summary of test results.

### 1.1. Test Specimens

Pipe specimens consisted of AWWA C900 polyvinyl chloride (PVC) (AWWA, 2007), AWWA C900 iPVC (AWWA, 2007), and AWWA C909 molecularly oriented polyvinyl chloride (PVCO) (AWWA, 2016). The connection under investigation is the RCT Flex-Tite coupling which is a self-restraining fitting with an integrated restraining gasket constructed primarily of ductile iron per ASTM A536. Flex-Tite fittings are pressure rated to 350 psi and available in a variety of tees, bends, and reducers, an example of which is provided in Figure 1.1. This program specifically examines the straight coupling and the results are intended to be representative of the connection between pipe and restrained gasket connection for any 150-mm (6-in.) diameter fitting configuration.



Available: <http://www.rctfittings.com/products/index.php>

Figure 1.1. Examples of the RCT Flex-Tite (a) coupling and (b) tee

## 1.2. Test Overview

All specimens tested were 6 in. (150 mm) diameter pipe, commercially available and conforming to C900 (PVC and iPVC) and C909 (PVCO) standards. Table 1.1 provides an overview of the test specimens and experiments performed. The Test ID represents the test type and a unique numerical value specific to the sequence of all testing performed at CIEST. Pipe-Connection identifies the pipe material connection type while Pipe Pressure Class refers to the class of the pipe material. Differences between DR14 and DR18 are primarily due to thicknesses of the pipe specimen. The approximate internal pressure at which the test was conducted is also included.

Table 1.1. Summary of Tests and Specimens

Test ID	Test description	Pipe-Connection	Pipe Pressure Class (psi)		Pipe Wall Thickness (in.)	Internal pressure (psi)
PT01	Axial Tension	iPVC - RCT	305	DR14	0.512	7
PT02	Axial Tension	iPVC - RCT	305	DR14	0.512	60
PT05	Axial Tension	PVCO - RCT	305	T800	0.315	65
PT09	Axial Tension	PVC - RCT	235	DR18	0.415	65
PC06	Axial Compression	PVCO - RCT	235	T600	0.268	65
PS12	Axial Cyclic	iPVC - RCT	305	DR14	0.512	63



## 2. General Test Setup and Protocols

This section is intended to provide a detailed overview of the setup procedure and key experimental constraints associated with application of axial load to water distribution pipelines. The intent is to expose the system to external loading conditions representative of the significant deformations possible during earthquake-induced ground deformation such as landslides, fault rupture, and liquefaction-induced lateral spreading, thus characterizing the pipeline system capacity. All tests were designed and performed in accordance with procedures and recommendations provided by Wham et al. (2018).

### 2.1. Axial Test Setup

This section outlines the test setup procedure for axial loading of a given pipe specimen. Figure 2.1 shows an image of the axial tension test setup and equipment. A 255.17 Materials Testing System (MTS) actuator, 110-kip load cell, and load frame were used to apply tensile and compressive load to the test specimen (Figure 2.2). The test specimens consisted of nominal 6 in (150 mm) diameter pipe with coupling.

#### 2.1.1. Specimen Installation Procedure

The pipe specimen is prepared at a length of approximately 13 ft (4 m) for tensile testing (two 78-in. (1980-mm) segments). The length varies depending on the loading direction (tension or compression) and coupling or joint under investigation. The pipe was cut using standard field installation practices outlined in appendix B. Measurements are provided at 0.5 in (13 mm) increments on the factory prepared pipe ends, which are inserted into the coupling or joint, as shown in Figure 2.3.

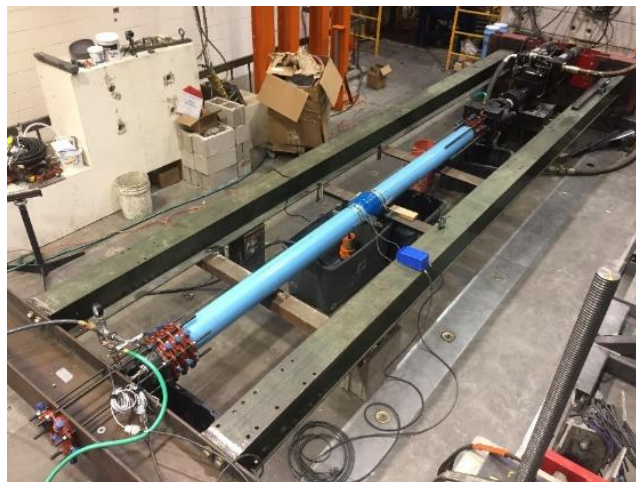


Figure 2.1. Pipe specimen in axial test frame

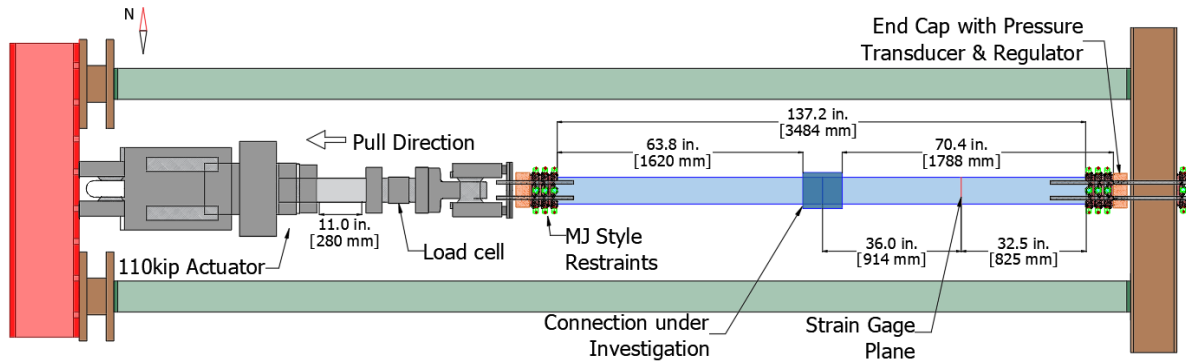


Figure 2.2. Dimensioned drawing of axial test setup



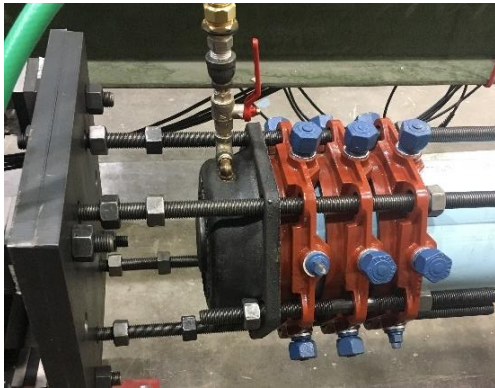
Figure 2.3. Marked measurements on non-cut ends of the pipe.



Figure 2.4. Identifying the pipe coordinates (crown, invert, springlines)

A level and crowning tool are used to identify the top (crown), bottom (invert), and spring lines of the pipe (Figure 2.4). Strain gauge planes are marked at approximately 36 in (910 mm) from either side of the specimen center line, as shown in Figure 2.2.

Three (3) 2006PV Megalug restraints are used at either end of the specimen to transfer the externally applied axial load. Figure 2.5 shows the restraints positioned at the loading (west) end and fixed (east) end of the specimen. The outer-most restraint for each end is aligned 2 in. (50 mm) from the end pipe and hand tightened into place. Each set of restraints are aligned with their respective end loading arrangements. The east side, fixed to the load frame, is positioned with a threaded rod located at the crown of the specimen, and the west side (actuator or loading side) is aligned with restraint nuts located at the crown. Two short threaded rods are used to pull the remaining two restraints into contact with the first, as shown in Figure



(a) Loading (west) end



(b) Fixed (east) end

Figure 2.5. Pipe connections to loading frame



Figure 2.6. Megalug restraints on “cut” ends of pipe

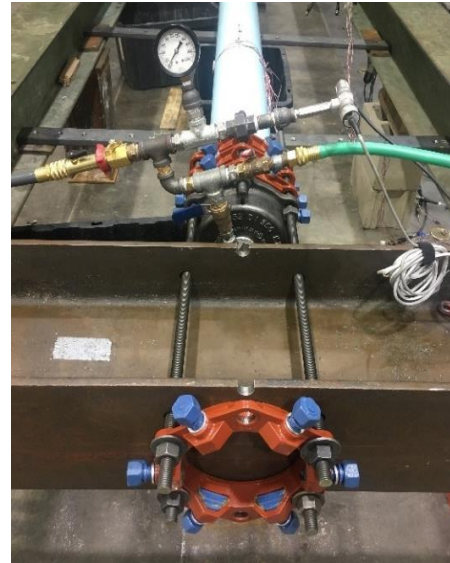


Figure 2.7. Fixed end (east) with water intake and pressure valve

2.6, two provide a composite 3-restraint end condition. The clamping nuts of the remaining Megalugs are then hand tightened into place.

The nuts on each end restraint are tightened in a star pattern using a torque wrench set to 30 ft-lbs (40.7 Nm). The torque wrench is then set to 60 ft-lbs (81 Nm) and the process is repeated until all restraints are secured to the pipe. While the Megalug restraint is equipped with self-torqueing, twist off clamping nuts for typical field installation, prior experience suggests that incrementally increasing torque provides a more uniformly distributed clamping force that ensures consistent circumferential contact and deters failure at the ends of the specimen.



Strain Gauges are installed at designated locations following the procedure outlined in “Strain Gauge Application Procedure” (see Appendix A) and additional details are included in the following section.

The specimen is then placed in the loading frame and the east and west connections were appropriately aligned with the actuator in its fully extended position (tension test) or fully retracted position (compression test). Lubrication (for the gasket to be used) is applied to the endcap gaskets and the inner diameter of the endcaps, the gasket is positioned against the outermost end restraint (as shown in Figure 2.6), and the endcaps are tightened in place with threaded rods (Figure 2.5). The east end cap is equipped with pressurization equipment including a water inlet (Figure 2.7) while the west endcap includes a bleeder valve at the crown to remove air during filling of the pipe. The elbow for the water intake on the east endcap and the air release valve on the west endcap are positioned vertically. Two short threaded rods on the crown and the invert (east) and on each spring line (west) are installed to secure the endcap to the pipe. On the east end, four 36 in (910 mm) long, 0.75 in (19 mm) diameter high-strength (120 ksi) threaded rods are installed to secure the pipe to the frame. Two nuts per rod are threaded during placement such that their final position is between the testing frame and the endcaps, as shown in Figure 2.5. A restraint is set into place over the four rods on the outer flange of the frame (Figure 2.7). Nuts and washers are then applied to each end to secure the pipe to the testing frame. A similar procedure was followed on the west end. Four 24 in (600 mm) long threaded rods are used to fix the specimen to a transfer plate machined with a hole pattern matching the restraints. The steel nuts and threaded rod connections are arranged such that axial force from pressurization is resisted by the actuator, and thus measured by the actuator load cell.

### ***2.1.2. Instrumentation***

Figure 2.8 shows a plan view of the tension test setup and key instrumentation. Four string potentiometers (string pots) or Linearly Varying Differential Transducers (LVDTs) were attached to the specimen at several locations to measure axial displacements. A string pot/LVDT is used at each end of the specimen to measure relative movement between the pipe specimen and end restraints. Two additional string pots/LVDTs were installed at the center of the specimen to measure localized relative displacement between the pipe and coupling. An electronic pressure transducer is installed on the east end to measure internal water pressure during the test.

A total of eight strain gauges are fixed to the exterior of the specimen at one of two planes, designated as SG+36 and SG-36, as shown in Figure 2.2. The plane locations are positioned approximately halfway between the joint restraint (specimen centerline) and gripping restraints. At either plane, the strain gauges are placed at the crown, east springline, invert, and west springline. Gauge plane SG+36 is positioned 36

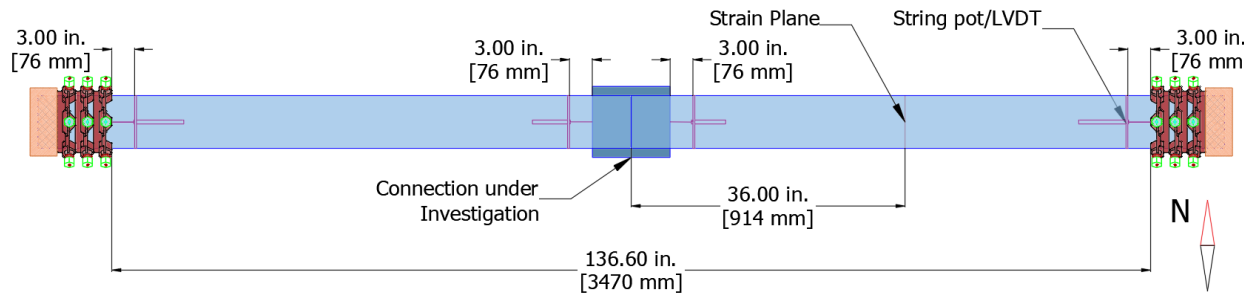


Figure 2.8. Specimen instrumentation

in. (910 mm) east of the specimen centerline and includes four x-y gauges, oriented in the axial and circumferential direction. Plane SG-36 was positioned 36 in. (910 mm) west of the specimen centerline and includes two x-y pairs located at the specimen springlines.

## 2.2. Test Procedure

The following section provides details of the test sequence, distributed into three parts: pretest, test sequence, and discussion of pause or stop criteria.

### 2.2.1. Pretest

Once the specimen is secured in the loading frame and the calibrated instrumentation is installed, the measuring systems are verified. The pipe is filled with water with the air bleed valve in the open position. The air bleed valve is closed once water has streamed from it and the system is pressurized to the laboratory pressure of approximately 65 psi (450 kPa) to check for leaks. Water is introduced into the specimen five hours or more before testing to ensure thermal acclimation to ambient laboratory conditions. Temperature readings of the external wall of the pipe are taken at several locations. Several pressurization sequences are completed to seat and verify readings of strain gauges and check axial force measured by the load cell. In each of the cycles the air bleed valve is opened to release any remaining air. Prior to a pressurization sequence, the nuts between the loading frame and the endcaps are tightened, such that when the pipe is pressurized, the axial pressurization force can be measured by the load cell. During the pressurization sequences, the pipe is pressurized to approximately 65 psi (450 kPa) and back down to 0 psi several times. After each sequence, data was collected, stored, and analyzed to ensure proper function of all measuring systems. The area surrounding the testing frame is cleared of all tools and other objects. Once ready for the test, a pretest meeting is conducted to review installation conditions, walk through instrumentation locations and expectations, and discuss safety equipment and concerns.



### ***2.2.2. Test Sequence***

After the pretest meeting is conducted and roles assigned, the test sequence is initiated by starting the data acquisition system and laboratory hydraulic systems. A data sampling rate of 4 Hz was used for all reported tests. The loading nuts at either end of the specimen are tightened to avoid any end movement due to pressurization. The appropriate water pressure is applied depending on the specific test. The test is performed under displacement control at a rate of 1 in. (25.4 mm) per minute. Displacement is applied until the specimen is no longer capable of holding internal water pressure or until the maximum stroke of the actuator [11 in. (280 mm)] is reached. Once the test is completed, the data acquisition system is turned off, laboratory hydraulic systems set to low pressure, and data is backed up.

### ***2.2.3. Stop or Pause Criteria***

Several predetermined interruptions to the test sequence are identified prior to testing. The test is paused if the specimen loses all water pressure during the test. If undesirable leakage occurs at the end caps they are tightened, and the test is resumed. If any leakage is observed at the coupling or center of the specimen, the test is paused briefly, leakage rate assessed, and the test resumed until ultimate failure. The test is paused if any fundamental instrumentation malfunctions during the test, or if power is lost in any part of the testing laboratory. The test is terminated when the specimen is unable to hold internal water pressure, which typically occurs as a result of structural failure of the pipe body or connection.



### 3. Axial Tension Results

The following section provides results from axial tension tests performed on different pipe materials. A total of four axial tension tests are reported in the following sections. For all tests, displacement was applied at a rate of 1 in. (25 mm) per minute.

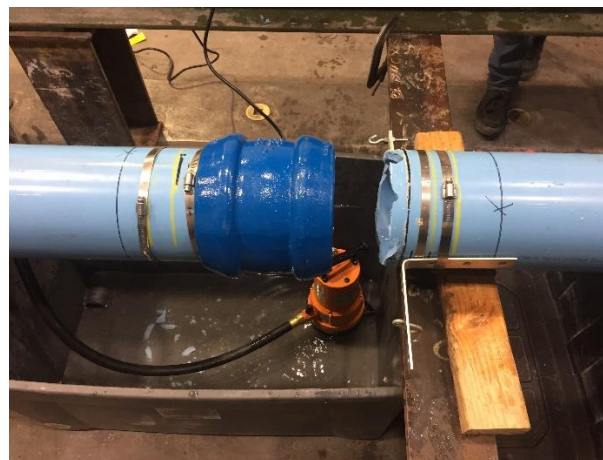
#### 3.1. Tension Test PT01 Results

The first axial tension test consisted of iPVC pipe with an RCT coupling at the midpoint. Figure 3.1 shows photos taken before the test and after specimen failure. As shown by the blue line in Figure 3.2, internal pressure for PT01 ranged between 0 and 7 psi (0 – 48 kPa), representing negligible water pressure. Figure 3.2 also shows actuator force and displacement relative to time during the test. The internal pressure fluctuation is a function of the increasing internal volume during applied tensile load and the pressure regulator's inefficiency at sustaining low levels of pressure. Note that pressure regulator performance was improved in subsequent tests and had negligible impact on PT01 test results.

Force vs. displacement plots of PT01 are provided in Figure 3.3 (a) and (b). The difference in displacement between the imposed actuator displacement and measured joint opening represents the stretch in the pipe combined with additional sources of slip and movement at either end restraint. The measurements of joint opening provide a localized representation of the relative movement between the coupling and pipe. Strain gages were not employed for this first tension test but are included in all subsequent tests. At an actuator displacement of 3.82 in. (97 mm) and an average joint opening of 0.89 in. (23 mm) PT01 reached a maximum axial force of 55.3 kips (246 kN), followed immediately by fracture of the specimen. No leakage or loss of water from the RCT connection was observed prior to ultimate failure. As shown in Figure 3.4,



(a)



(b)

Figure 3.1. Specimen PT01 (a) before and (b) after axial tension test



the specimen failed by circumferential fracture at the stress concentrations imposed by the RCT's serrated teeth digging into the pipe wall.

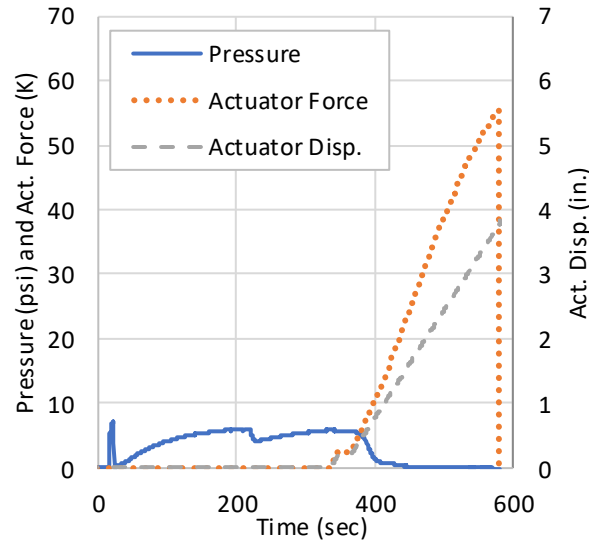


Figure 3.2. PT01 results for internal pressure, actuator displacement and axial force vs. time

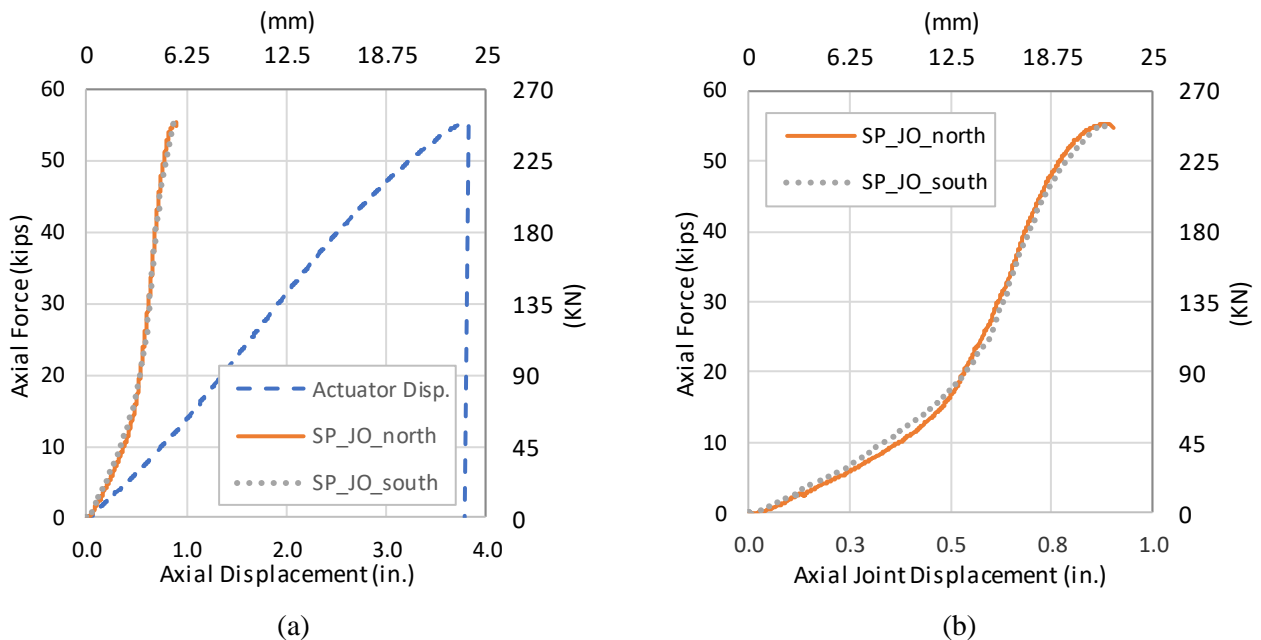
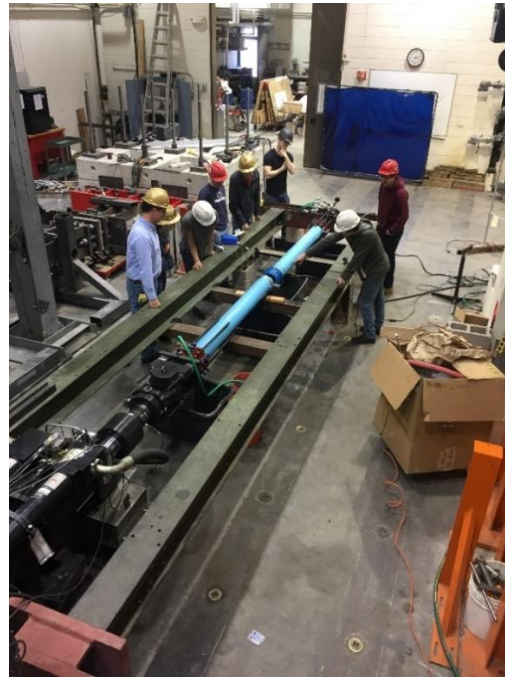


Figure 3.3. Specimen PT01 actuator force vs. (a) measured axial displacements and (b) total joint displacement at north and south springline string pots



(a)



(b)

Figure 3.4. Specimen PT01 after failure: (a) circumferential fracture and (b) test overview

### 3.2. Tension Test PT02 Results

The second axial tension test, PT02, was performed on iPVC pipe with an RCT coupling at the midpoint. Figure 3.5 provides photos taken before and after the test. Figure 3.6 shows the progression of pressure, actuator force and displacement over time while Figure 3.7 shows actuator force vs. actuator displacement. Actuator displacement and force are direct measurements of the hydraulic actuator piston and inline load cell, respectively. Displacement was applied at a rate of 1 in. (25 mm) per minute, and the force feedback of the load cell was recorded. The maximum axial force recorded in the load cell was 55.3 kips (246 kN) at an actuator displacement of 3.82 in. (97 mm). There was some leakage in the endcaps during the test, which resulted in a few pauses to regain a constant internal water pressure. Although there were some fluctuations in internal pressure during the test, the average sustained pressure during loading was approximately 60 psi (414 kPa) and failure occurred at 56.3 psi (388 kPa).

Figure 3.8 shows the actuator force vs. the joint displacement. Joint displacement was measured using two string potentiometers located on the north and south springline, measuring across the RCT coupling, shown in Figure 3.5(a). The north string potentiometer began slipping at about 0.5 in. (12.7 mm) of joint displacement, after which data was unreliable and removed from the figure. The joint displacement on the



Figure 3.5. Specimen PT02 (a) before and (b) after axial tension test

south springline recorded 0.92 in (23 mm) just before failure. Failure occurred on both sides of the RCT coupling simultaneously, shown in Figure 3.5 (b).

Figure 3.9 shows the average axial and circumferential strains for the duration of the test. At a time of about 50 seconds into data acquisition, the system was fully pressurized, and an increase in circumferential strain was observed. Once loading began at about 175 seconds, the circumferential strains began to decrease, while the axial strains increased. As the actuator applied tensile loading to the system, the pipe began to elongate, causing an increase in axial strains. Due to Poisson's effect, the circumferential strain

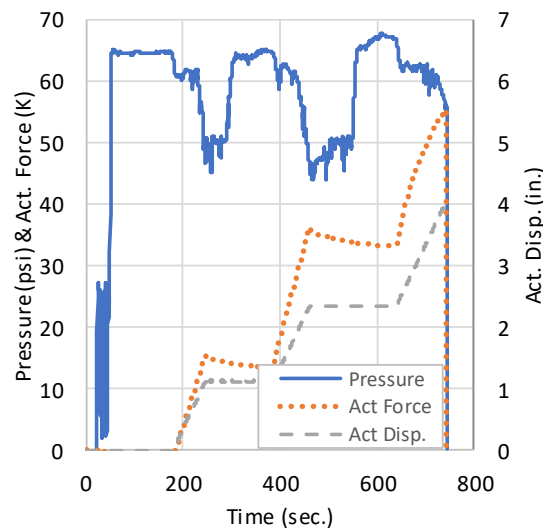


Figure 3.6. PT02 pressure, axial load, and actuator displacement vs. time



decreased as tensile load was applied. The magnitude of the measured axial strains shown in Figure 3.9 was determined, after the test was completed, to be inaccurate. A measuring error associated with the axial strain gauge calibration occurred. The authors anticipate the strain gauges to measure approximately 60% greater strain at failure, similar to the results gained from the cyclic test reported in Section 5 of this report. The strains are reported herein to illustrate the trends imposed during the test.

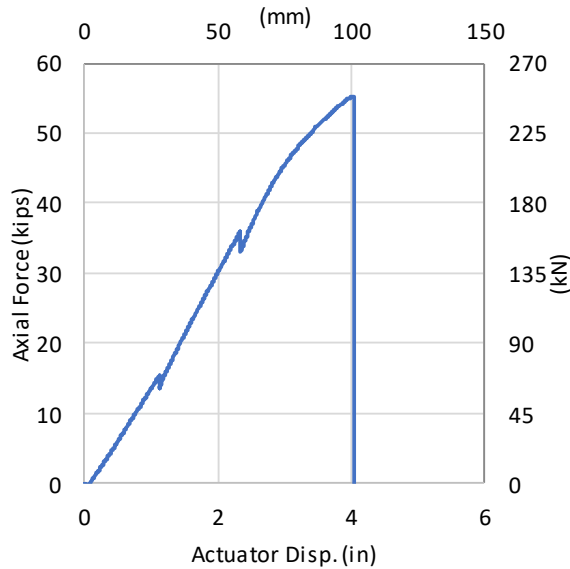


Figure 3.7. PT02 Axial Force vs Actuator Displacement

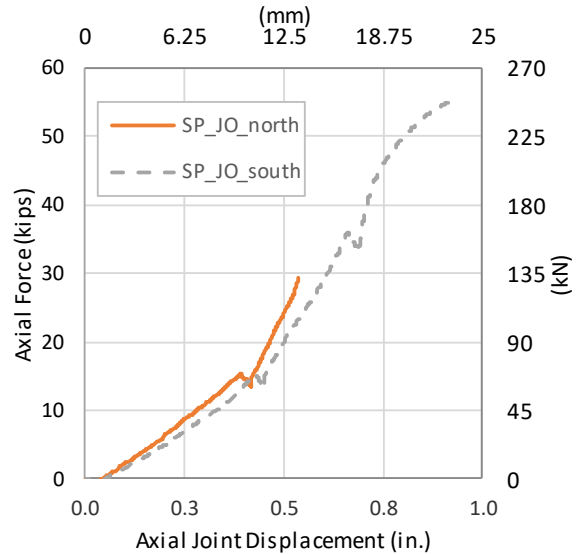
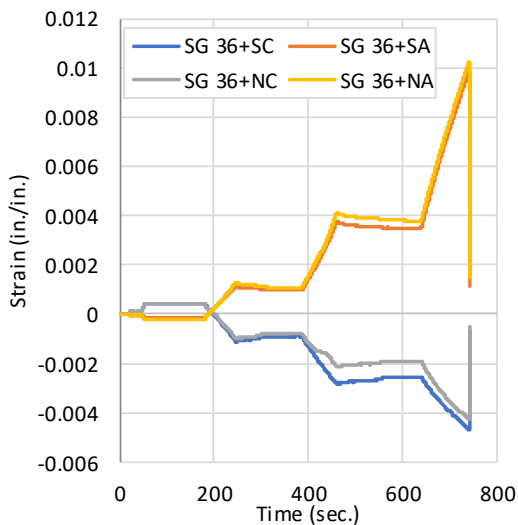
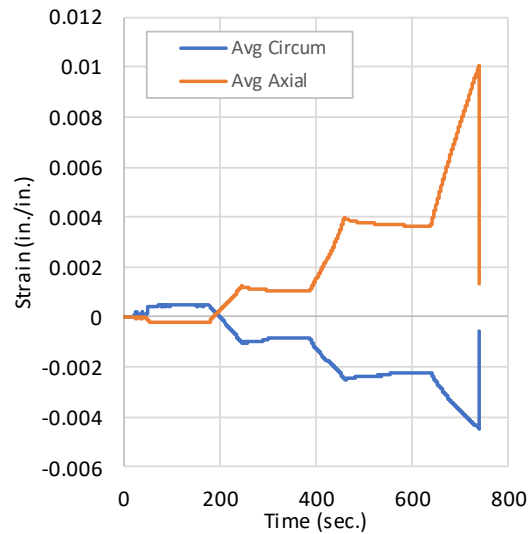


Figure 3.8. PT02 Force vs Joint Displacement



(a) Measured strains vs. time



(b) Average strains vs. time

Figure 3.9. PT02 axial and circumferential strains



### 3.3. Tension Test PT05 Results

Molecularly oriented PVC (PVCO) pipe with an RCT coupling was used for this test. Figure 3.10 shows the relationship between actuator force, internal pressure, and actuator displacement vs time. Actuator forces and displacements are direct measurements of the actuator load cell and piston, respectively. Displacement was applied at a rate of 1.0 in./min. (25 mm/min.), and the force feedback of the load cell was recorded. Figure 3.11 shows the maximum force recorded in the load cell was 27.8 kips (124 kN) at an actuator displacement of 2.9 in. (74 mm). There was no leakage of the endcaps throughout the duration of the test, which resulted in a constant internal water pressure of about 63 psi (434 kPa).

Figure 3.12 shows the actuator force vs. various displacement measures. Displacements between the pipe and end restraints (Megalugs in series) at either end of the specimen, denoted by “east end” and “west end” in the figure, indicate relatively minor movement [ $<0.25$  in. (6.4 mm)] at the fixed ends. Joint displacement was measured using two LVDTs located at either end of the coupling, and one string potentiometer along the north springline, shown in Figure 3.13. The joint displacement reached an average of about 0.73 in (18 mm) just before failure. Each of the LVDTs measured relative joint displacement for each side of the RCT coupling, which were summed to calculate the total joint displacement. This value was checked against the string potentiometer measurement, resulting in reasonably consistent values. Failure occurred on the West side of the coupling, fracturing at the contact point between the pipe and the coupling, shown in Figure 3.14.

Figure 3.15 shows the average axial and circumferential strains for the duration of the test. At a time of about 20 seconds into data acquisition, the system was fully pressurized, and an increase in circumferential

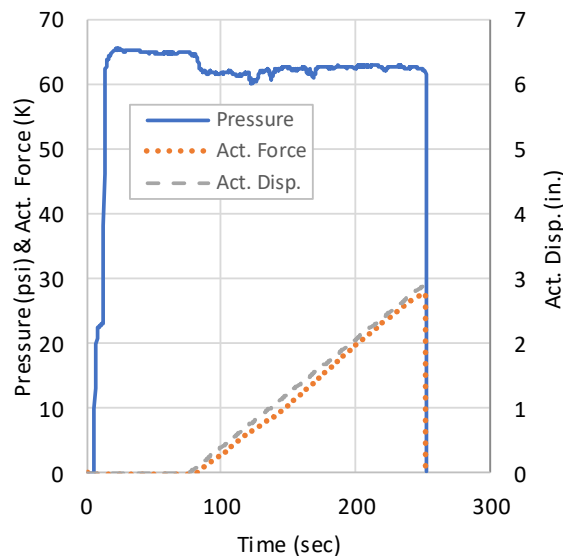


Figure 3.10. Specimen PT05 results for pressure, axial force, and actuator displacement vs. time

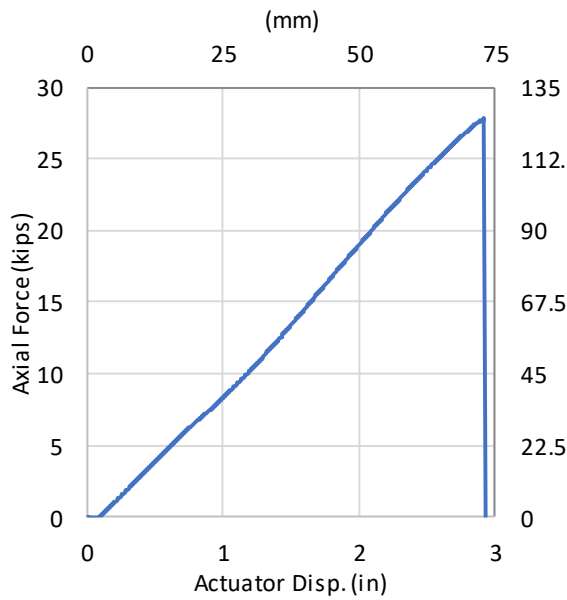


Figure 3.11. PT05 Force vs Actuator Displacement

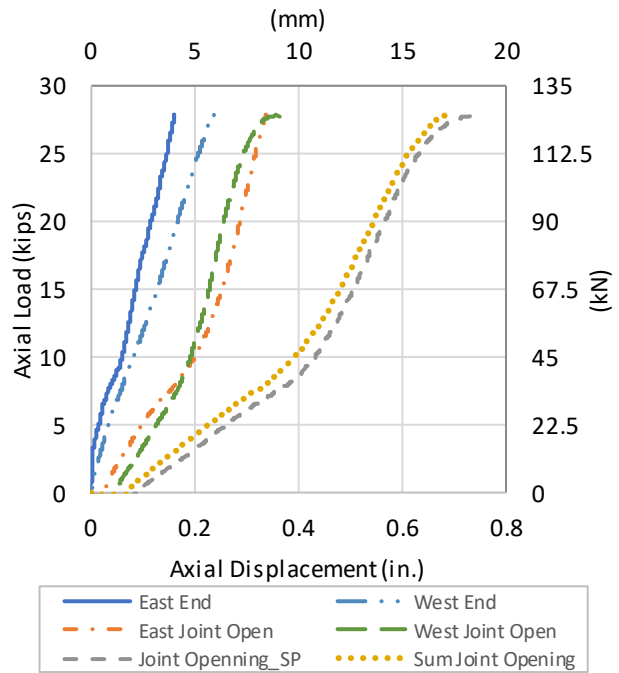


Figure 3.12. PT05 Force vs Joint Displacements

strain was observed. Once loading began at about 80 seconds, the circumferential strains began to decrease, while the axial strains increased. As the actuator applied tensile loading to the system, the pipe began to elongate, causing the increase in axial strains. However, due to Poisson's effect, the circumferential strain decreased as the tensile load was applied. The maximum axial strain was measured at about 1.17% prior to failure.



Figure 3.13. LVDTs (top) and string potentiometer (bottom) locations for PT05

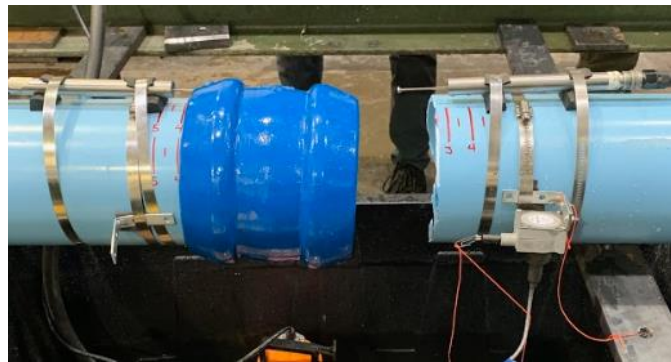


Figure 3.14. Failure at east joint for PT05

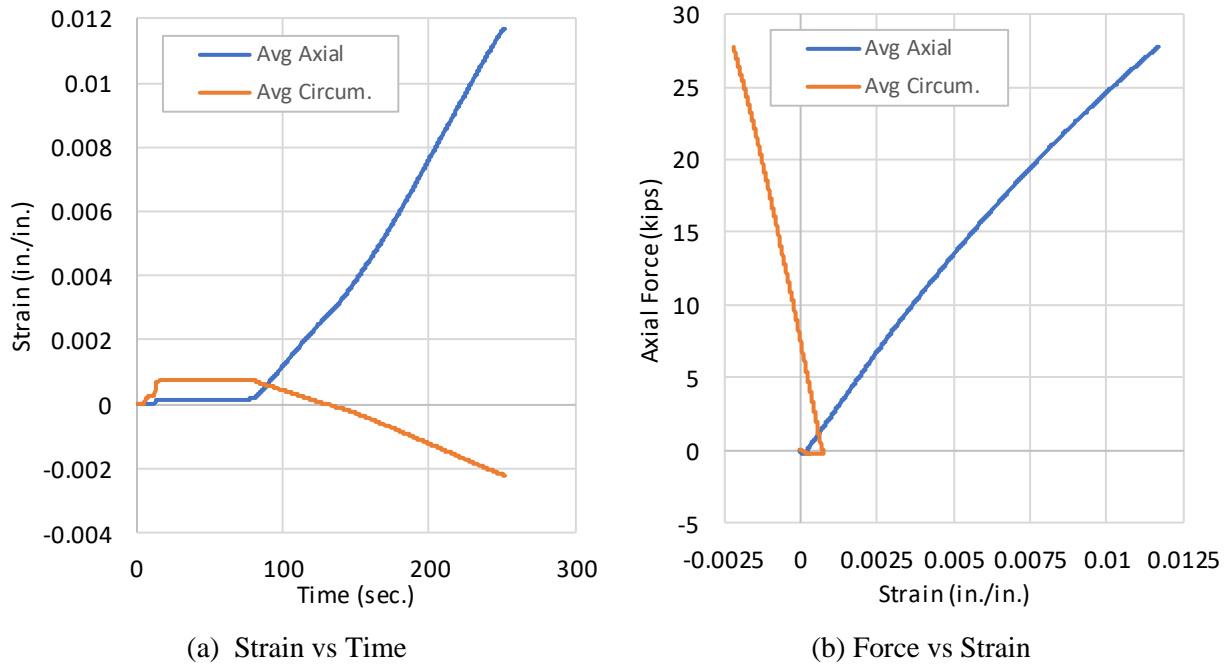


Figure 3.15. PT05 Average axial and circumferential strains vs. (a) time and (b) axial force

### 3.4. Tension Test PT09 Results

PVC C900 standard pipe with an RCT coupling restraint was used for test PT09. Figure 3.16 shows the relationship among actuator force, internal pressure, and actuator displacement. Actuator forces and displacements are direct measurements of the hydraulic load cell and piston, respectively. Displacement

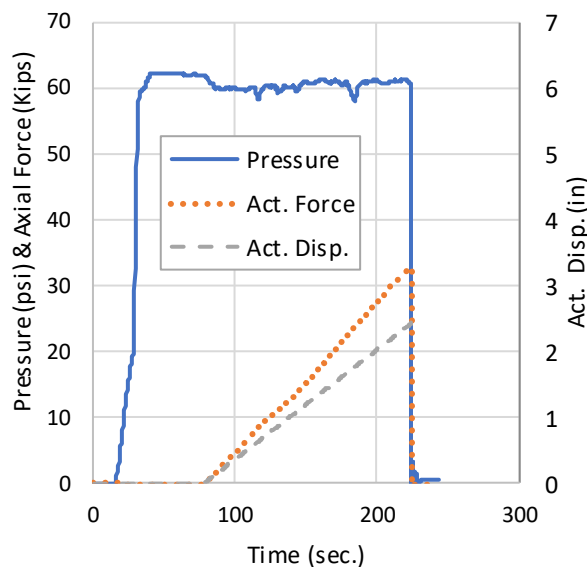


Figure 3.16. Specimen PT09 results for pressure, axial force, and actuator displacement vs. time



was applied at a rate of 1.0 in./min. (25 mm/min.), and the force feedback of the load cell was recorded. Figure 3.17 shows that the maximum force recorded in the load cell was 32.8 kips (146 kN) at an actuator displacement of 2.43 in. (61 mm). There was no leakage of the endcaps during the duration of the test, which resulted in a constant internal water pressure of about 63 psi (434 kPa). Figure 3.18 shows the actuator force vs. the joint displacement. Joint displacement was measured using two LVDTs located on both ends of the coupling, shown in Figure 3.19. The joint displacement reached an average of about 0.54 in (14 mm) just before failure. Each of the LVDTs measured relative joint displacement for each side of the RCT coupling, which were summed to calculate the total joint displacement. Failure occurred on the East side of the coupling, fracturing at the contact point between the pipe and the coupling, shown in Figure 3.20.

Figure 3.21 shows the average axial and circumferential strains for the duration of the test. At a time of about 30 seconds into data acquisition, the system was fully pressurized, and an increase in circumferential strain was observed. Once loading began at about 80 seconds, the circumferential strains began to decrease, while the axial strains increased. As the actuator applied tensile loading to the system, the pipe began to elongate, causing the increase in axial strains. However, due to Poisson's effect, the circumferential strain decreased as the tensile load was applied. The maximum axial strain was measured at about 1.0% prior to failure.

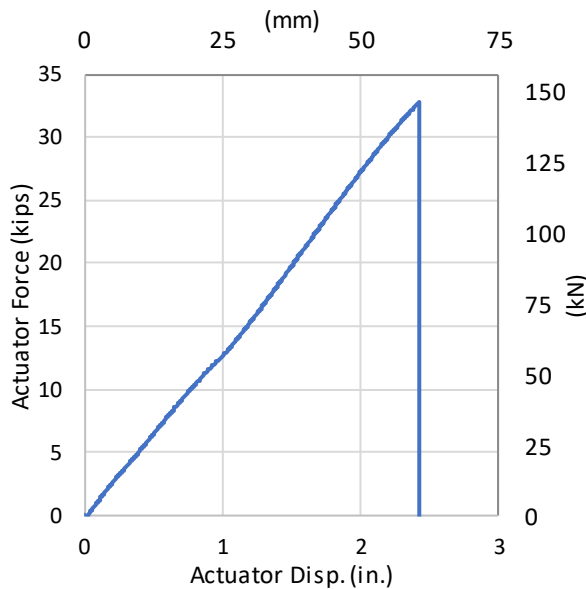


Figure 3.17. PT09 Force vs Actuator Displacement

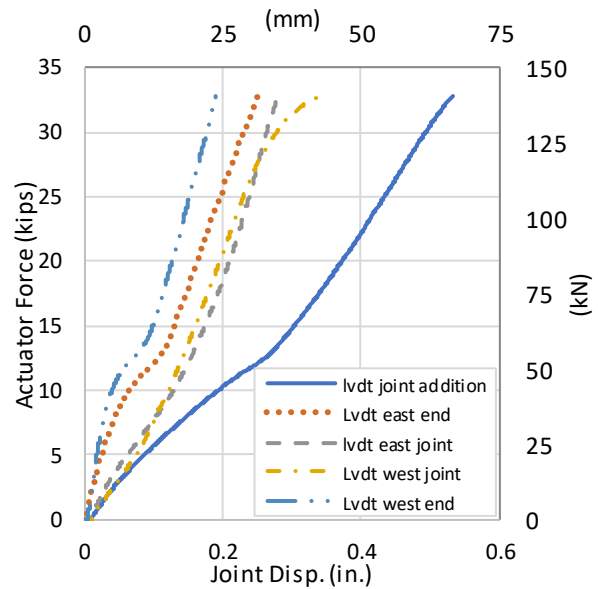


Figure 3.18. PT09 Force vs Joint Displacements



Figure 3.19. LVDT locations for PT09

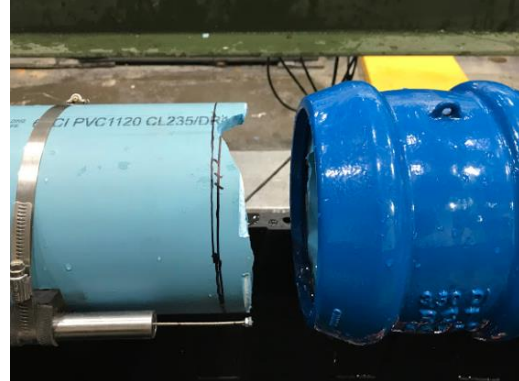
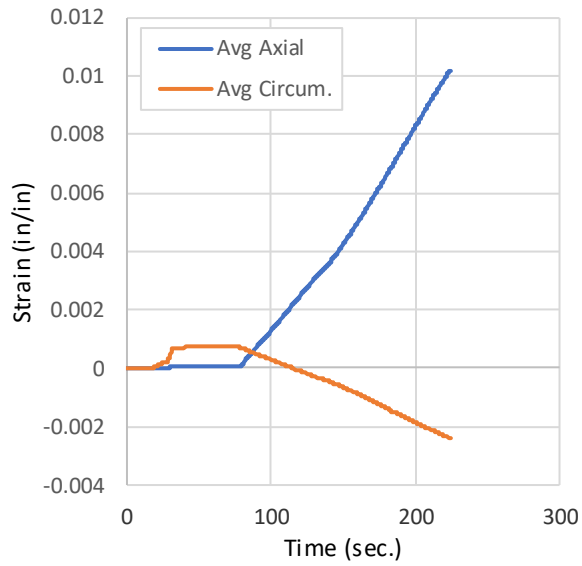
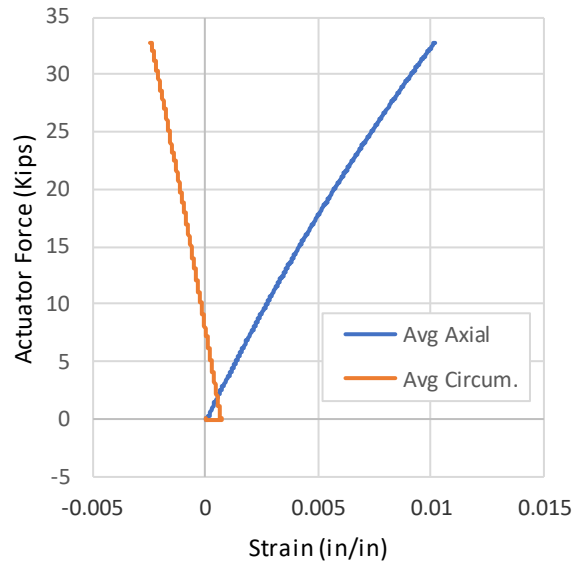


Figure 3.20. Failure at west joint for PT09



(a)



(b)

Figure 3.21. PT09 Average axial and circumferential strains vs. time and axial force



### 3.5. Comparison of Tension Test Results

This section compares results from the four tension tests performed on various materials and at a range of internal pressures. Table 3.1 outlines the different tests completed and their associated results.

Table 3.1. Summary of Axial Tension Test Results

Test # (CIEST)	Pipe- Connection	Max Axial Force		Max Axial Strain		Max Act. Disp.		Joint Disp.	
		kips	(kN)	in./in.	%	in.	(mm)	in.	(mm)
PT01	iPVC - RCT	55.3	(246)	NA	NA	3.820	(97)	0.893	(23)
PT02	iPVC - RCT	55.3	(246)	NA	NA	4.058	(103)	0.930	(24)
PT05	PVCO - RCT	28.0	(125)	0.0117	1.17	2.956	(75)	0.704	(18)
PT09	PVC - RCT	33.0	(147)	0.0102	1.020	2.472	(63)	0.533	(14)

Figure 3.22 shows the relationship between the axial force and the actuator displacement for all four tensions tests. Results from the iPVC were very consistent in both the low and high-pressure test. Each test resulted in a maximum force of 55.3 kips (246 kN), show in Figure 3.22. The PVCO and PVC recorded maximum forces of 28 and 33 kips (125 and 147 kN), respectively. Although the PVCO did not record as high of a force, it reached a higher actuator and joint displacement of 2.96 in (75 mm) and 0.70 in (18 mm), respectively, as opposed to the PVC, which recorded an actuator displacement of 2.47 in (63 mm) and a joint displacement of 0.53 in (14 mm).

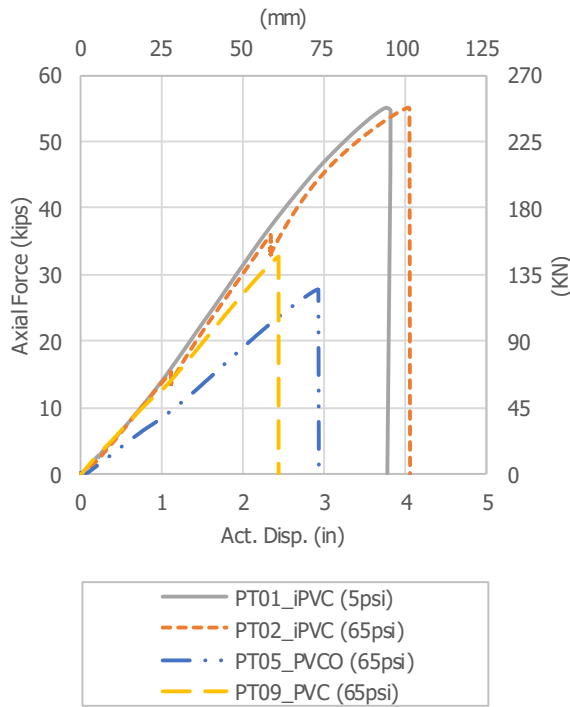


Figure 3.22. Tension Test Comparison for Axial Force vs Act. Disp.

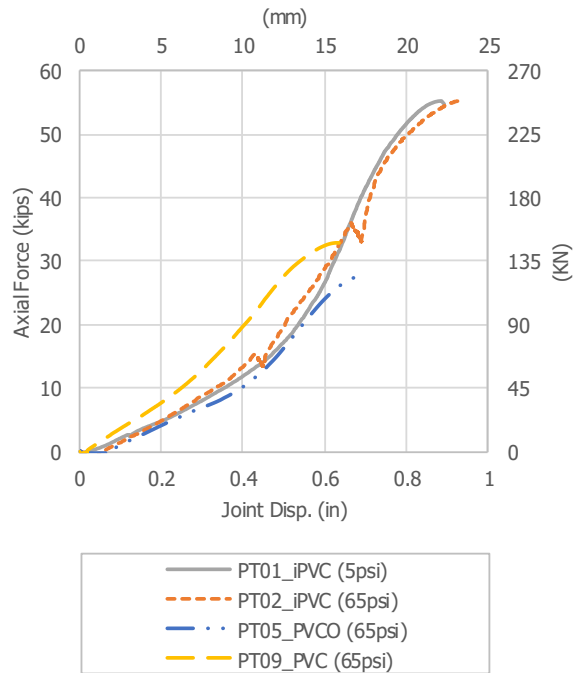


Figure 3.23. Tension Test Comparison for Axial Force vs Joint Disp.

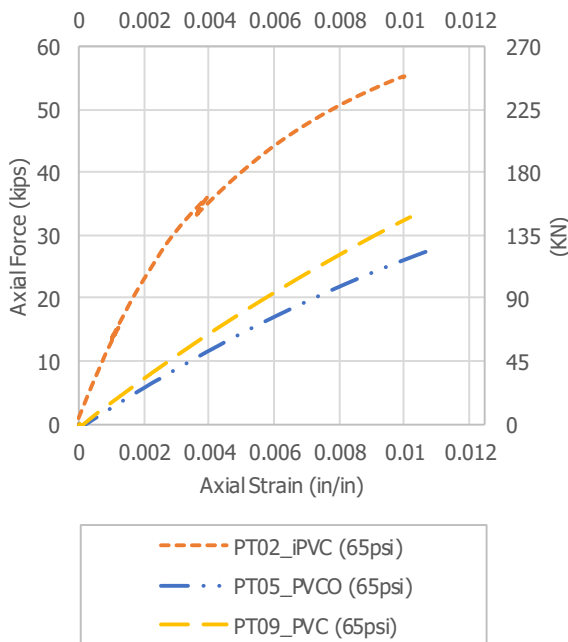


Figure 3.24. Tension Test Comparison for Axial Force vs Axial Strain. [Note PT02 measured strain is inaccurate]

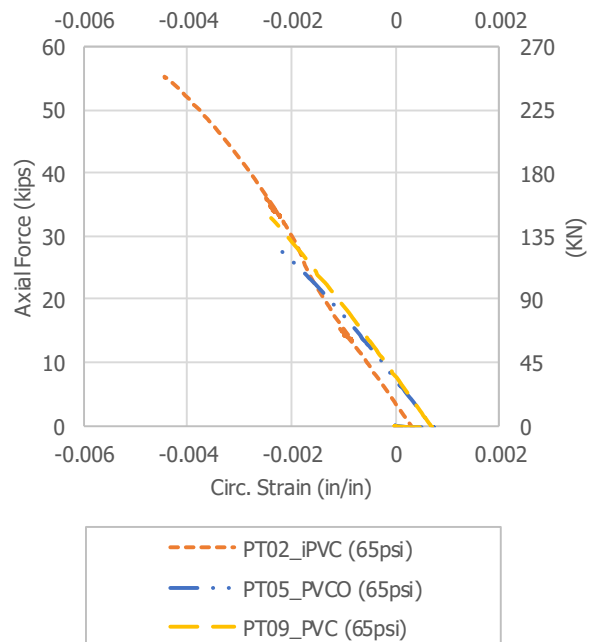


Figure 3.25. Tension Test Comparison for Axial Force vs Circ. Strain.



#### 4. Axial Compression Test

One axial compression test was conducted and reported herein. The compression test was setup similarly to the tension test, shown in Figure 4.1. The setup varied from the previously reported tension tests in the following ways. Lateral supports were provided to limit out-of-plane (global) buckling of the specimen. End restraints were orientation opposite of the tension tests (as shown in Figure 4.2) to mobilize the needed loading direction of Megalug end restraints. The specimen was approximately 12 in. (300 mm) longer to reduce the buckling length of the threaded rods while the stroke of the piston (11.2 in.) was fully retracted.



Figure 4.1. Compression test setup



Figure 4.2. Megalug end restraint orientation for compression

##### 4.1. Compression Test PC06 Results

Compression test PV06 was performed on a PVCO pipe with an RCT coupling at its center. Figure 4.3 shows the relationship among actuator force, internal pressure, and actuator displacement. Actuator forces and displacements are direct measurements of the hydraulic load cell and piston, respectively.

Displacement was applied at a rate of 1.0 in./min. (25 mm/min.), and the force feedback of the load cell was recorded. Compressive forces and displacements are taken as positive values during this section.

Figure 4.4 shows that the maximum force recorded in the load cell was 16.2 kips (146 kN) at an actuator displacement of 3.1 in. (79 mm) and the maximum displacement recorded was 7.06 in (61 mm). Due to bending in the specimen, the maximum force and displacement did not occur at that same time. Pressure varied throughout the test, as reduced volume caused spikes in the pressure that needed to be manually released throughout the procedure. The average pressure was about 63 psi (434 kPa) but ranged from 30 to 100 psi (207 to 690 kPa). Figure 4.5 shows the actuator force vs. joint displacement. Joint displacement was measured using two LVDTs located at either end of the coupling, and a string pot placed on the north springline, shown in Figure 4.6. However, severe buckling at the joint led to removal of the LVDTs during the test, which left only the string pot measurements. The maximum joint displacement was 2.2 in (56 mm). Buckling occurred at the contact point between the pipe and the coupling, shown in Figure 4.7. The test was stopped prior to failure due to instabilities caused by the knuckle of the actuator.

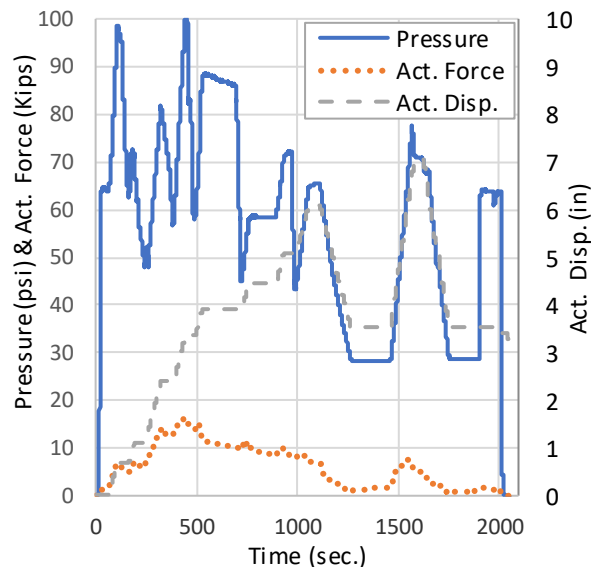


Figure 4.3. Specimen PC06 results for pressure, axial force, and actuator displacement vs. time

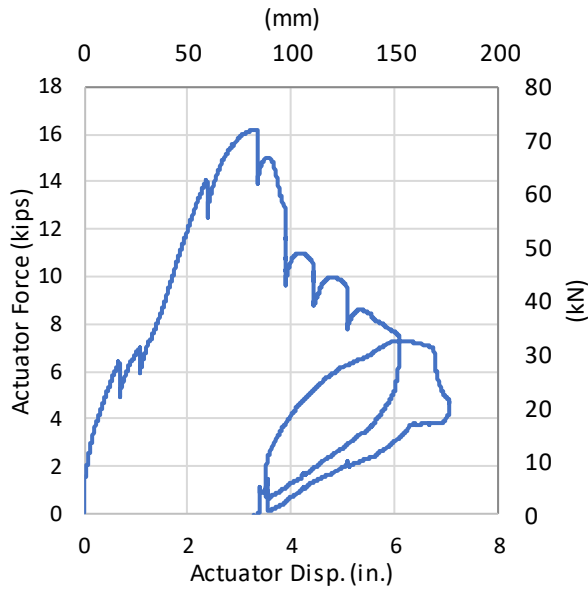


Figure 4.4. PC06 Force vs Actuator Displacement

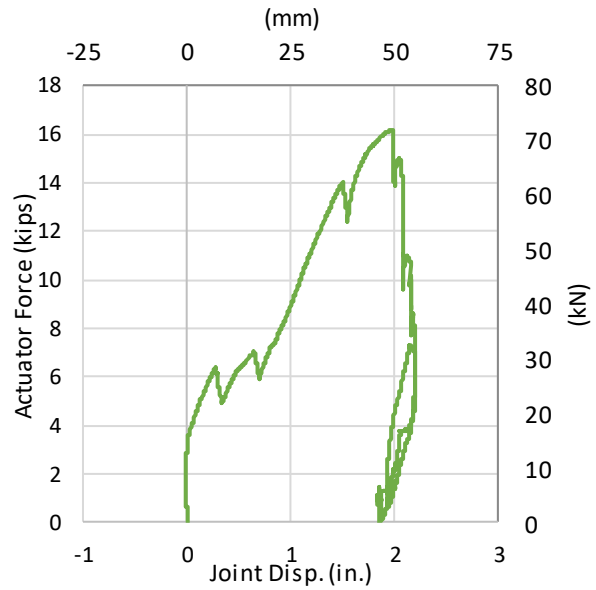


Figure 4.5. PC06 Force vs Joint Displacements



Figure 4.6. LVDT and String Potentiometer locations for PC06

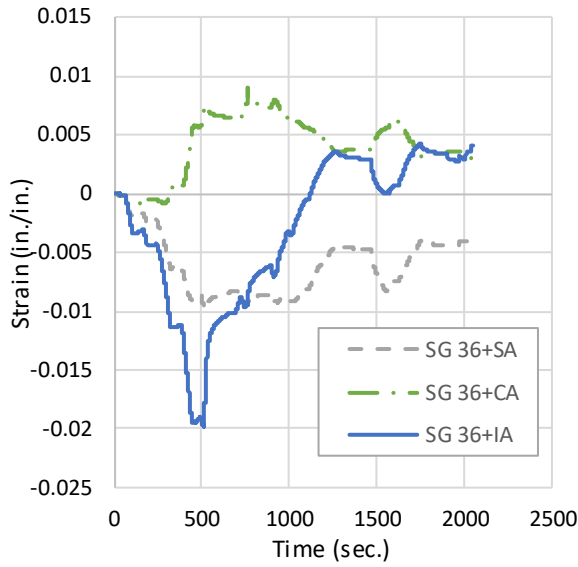


Figure 4.7. Buckle at east joint for PC06

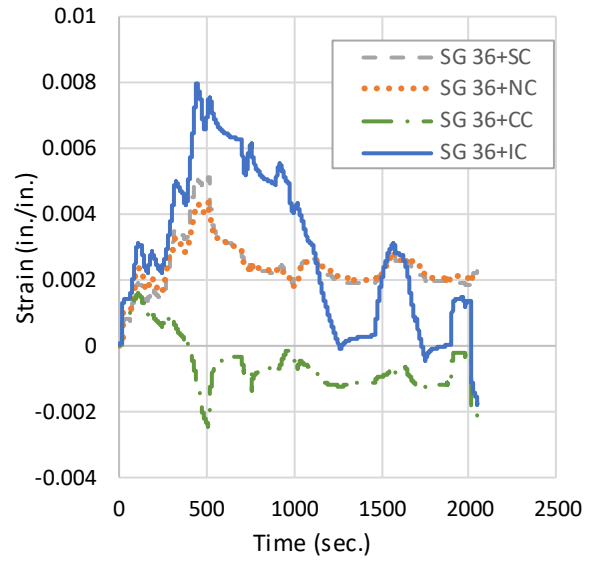
Figure 4.8 shows the axial and circumferential strains for the duration of the test. The axial strain gage placed on the north spring line did not record data during the test. Due to bending of the pipe, axial strains recorded on the crown were positive (elongated) and axial strains on the invert were negative (compressed). There is an inverse relationship between the axial strain circumferential strains due to Poisson's effect. Figure 4.9 shows the progression of the compression test at four instances in time. The specimen experienced progress out of plane buckling, which is represented by the widely varying strain



measurements. Despite significant levels of imposed actuator compression, the coupling performed well and did not experience leakage or ultimate failure.



(a) axial strains

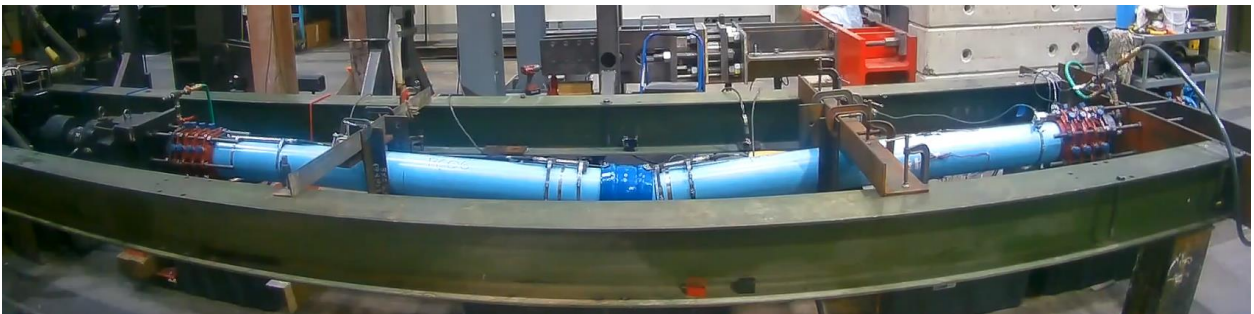


(b) circumferential strains

Figure 4.8. PC06 axial strain (a) and circumferential strain (b) vs. time



(a) Initial condition



(b) Mid-loading



(c) Max loading



(d) Unloaded

Figure 4.9. Images of PC06 loading progression

## 5. Axial Cyclic Tests

One axial cyclic test was conducted and reported herein. The cyclic test was setup identical to the compression test, generally depicted in Figure 4.1. This setup was used to account for the compressive loads during the cyclic motions, and does not interfere with the tension loading on the specimen. A balanced Megalug pattern (alternating directions) was used on the end restraints to ensure that both tensile and compressive loads could be accounted for, shown in Figure 5.1.

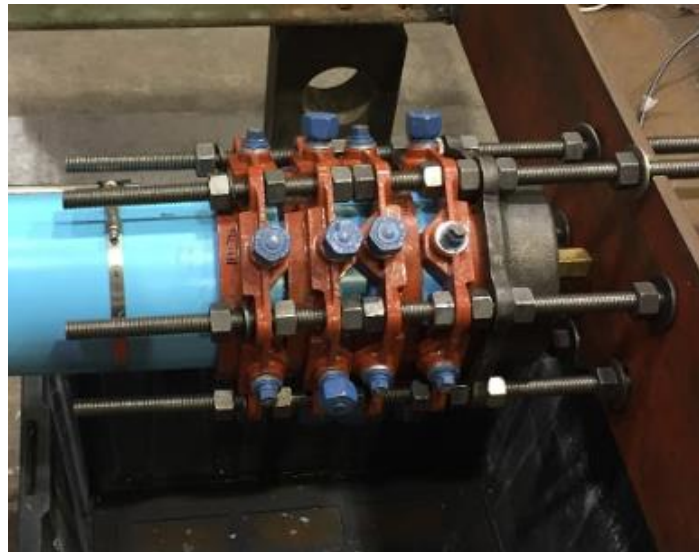


Figure 5.1. Megalug end restraint orientation for cyclic loading

### 5.1. Cyclic Test PS12 Results

The cyclic test was performed on an iPVC pipe with an RCT coupling at its center. The intention of this test was to determine if a reduction in maximum tensile joint strength occurs as a result of cyclic loading levels in excess of those could be imposed by transient wave propagation. Figure 5.2 shows the relationship among actuator force, internal pressure, and actuator displacement. Actuator forces and displacements are direct measurements of the hydraulic load cell and piston, respectively. Force-controlled loading was applied following guidelines of FEMA461, which discusses seismic load protocols for structural and nonstructural building components (Applied Technology Council, 2007). FEMA 461 maximum compressive load of 20 kips (89 kN). Following fifteen increments of force-controlled axial tension/compression load, the hydraulic system was switched to displacement control, and the specimen was pulled in tension at a rate of 1.0 in./min. (25 mm/min.) until failure. Figure 5.3 shows that the maximum force recorded in the load cell was 52.4 kips (233 kN) at a maximum displacement of 3.66 in (92 mm). Pressure varied throughout the test, as reduced volume caused spikes in the pressure that needed to be



manually released throughout the duration of the test. The average pressure was about 63 psi (434 kPa) but ranged from 50 to 75 psi (345 to 517 kPa). Figure 5.4 shows the actuator force vs. the joint displacement. Joint displacement was measured using two LVDTs located on both ends of the coupling, shown in Figure 5.5. The joint displacement was measured at 0.82 in (21 mm). Failure occurred at both contact points between the pipe and the center coupling, shown in Figure 5.6.

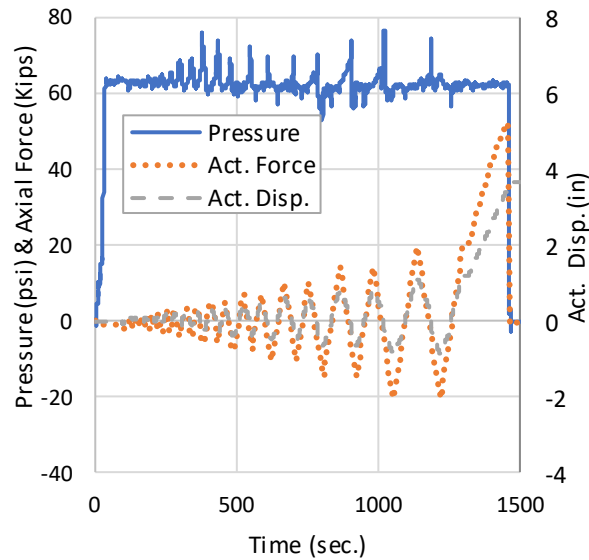


Figure 5.2. Specimen PS12 results for pressure, axial force, and actuator displacement vs. time

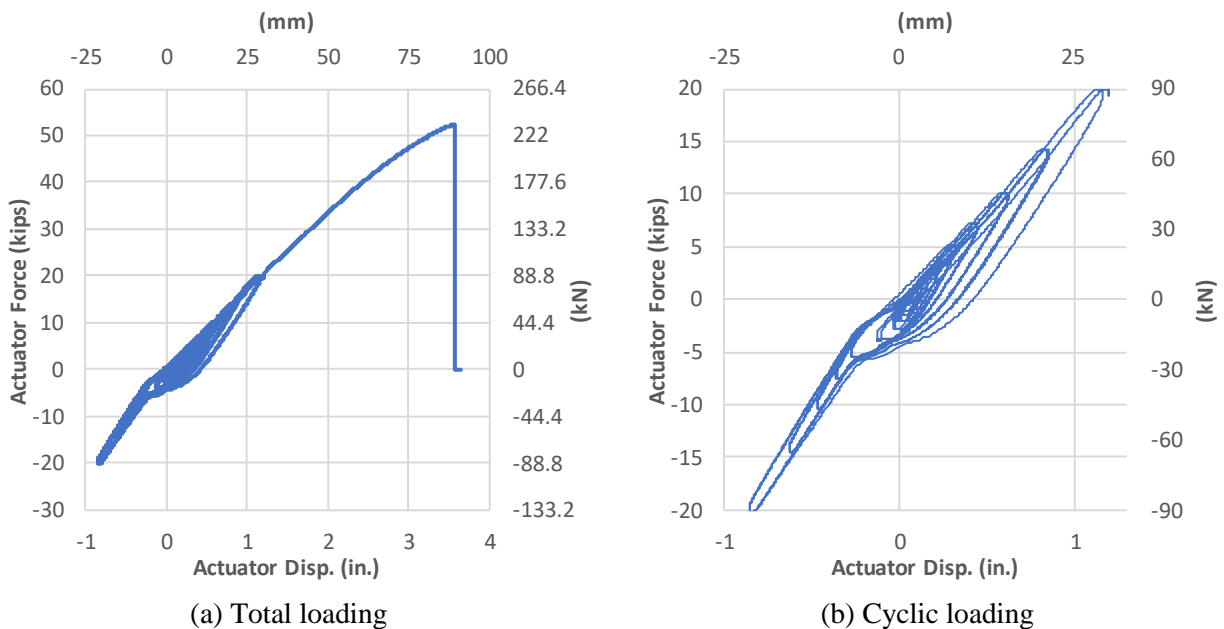


Figure 5.3. PS12 force vs actuator displacement

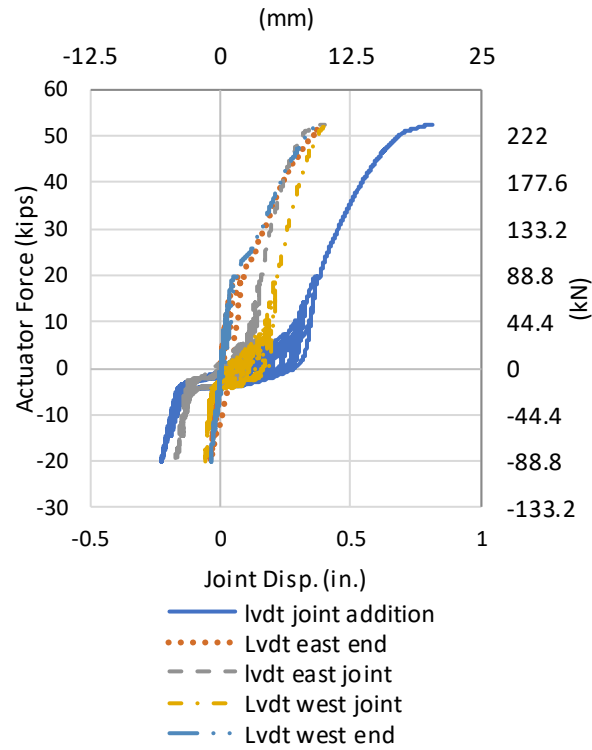


Figure 5.4. PS12 force vs axial displacements



Figure 5.5. LVDT locations for PS12



Figure 5.6. Failure at joint for PS12

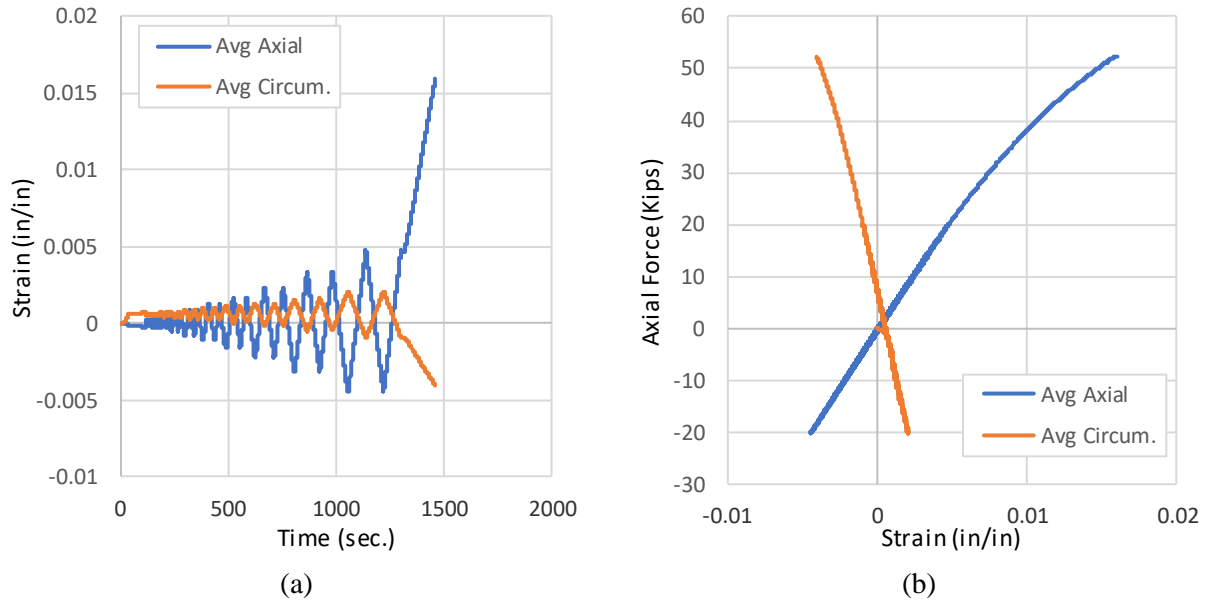


Figure 5.7. PS12 axial strain (a) and circumferential strain (b) vs. time

Figure 5.7 shows the axial and circumferential strains for the duration of the test. There is an inverse relationship between the axial strain circumferential strains due to Poisson's effect. The maximum axial strain was recorded at 1.6%.

## 5.2. Cyclic Test Comparison

This section provides comparison of the cyclic test to the axial tension tests, all performed on PC 305 iPVC pipe. Figure 5.8 shows excellent agreement among actuator force vs. displacement, with the cyclic test reaching a marginally reduced level of force and displacement. Similarly, Figure 5.9 shows the maximum joints displacement between cyclic and monotonic tests was similar, however the cyclic joint displacement follows a stiffer response. This stiffer response is likely due to moderate scraping of the restraining teeth along the pipe wall during the initial cyclic sequences. Although the response varies, the maximum obtained values suggest the cyclic displacements did not have a significant effect on the ultimate performance of the system. The axial strain comparison, shown in Figure 5.10, suggest some variation in axial strain development among the thermoplastic materials. The PVC and PVCO material reached similar levels of axial strain at failure with the PVC material exhibiting a stiffer initial response and the PVCO reaching greater total strain. Figure 5.11 shows excellent agreement amount circumferential strains in response to axial loading.

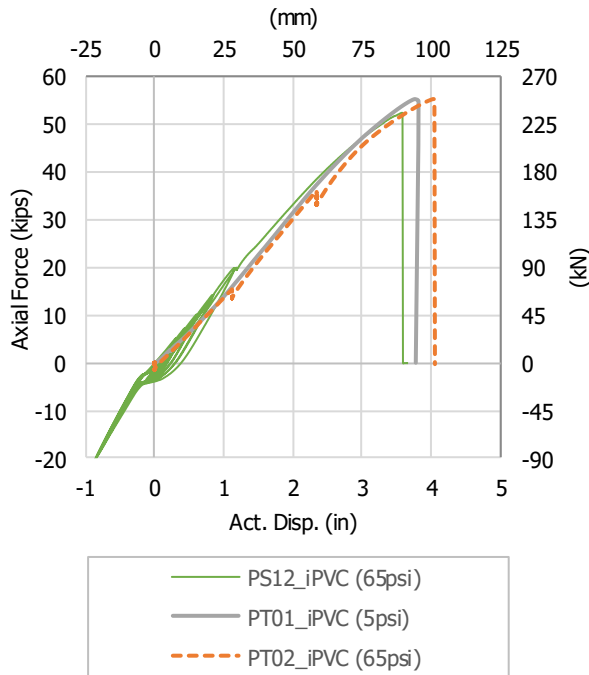


Figure 5.8. Tension Test Comparison for Axial Force vs Act. Disp.

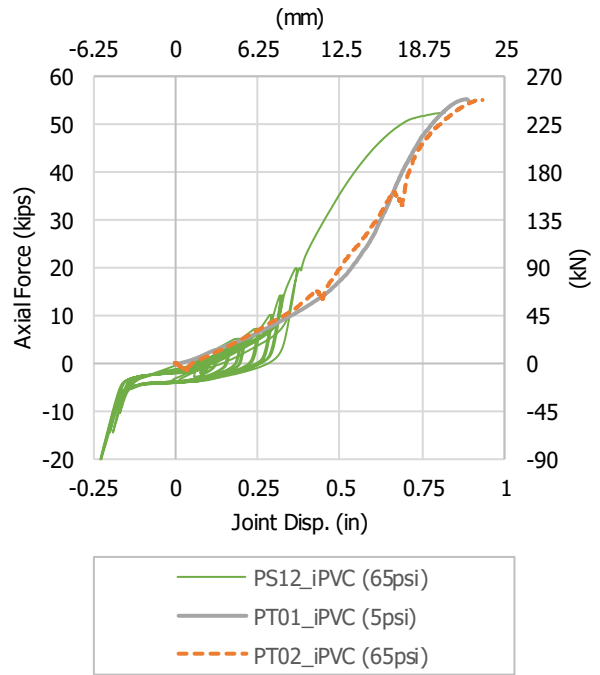


Figure 5.9. Tension Test Comparison for Axial Force vs Joint Disp.

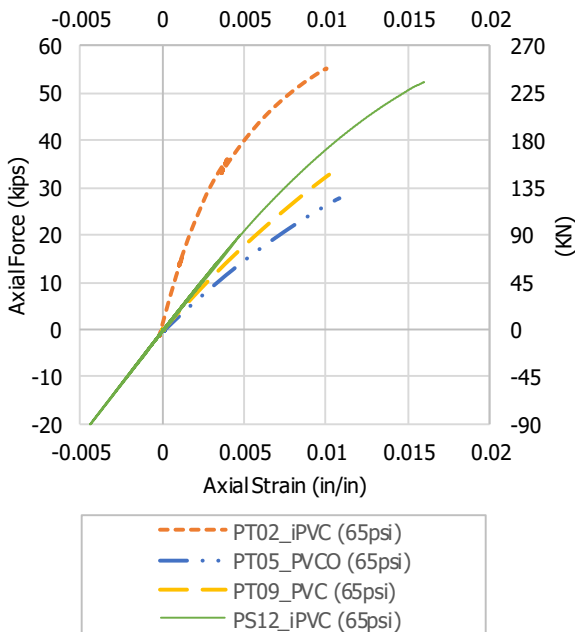


Figure 5.10. Tension Test Comparison for Axial Force vs Axial Strain. [Note PT02 measured strain is inaccurate]

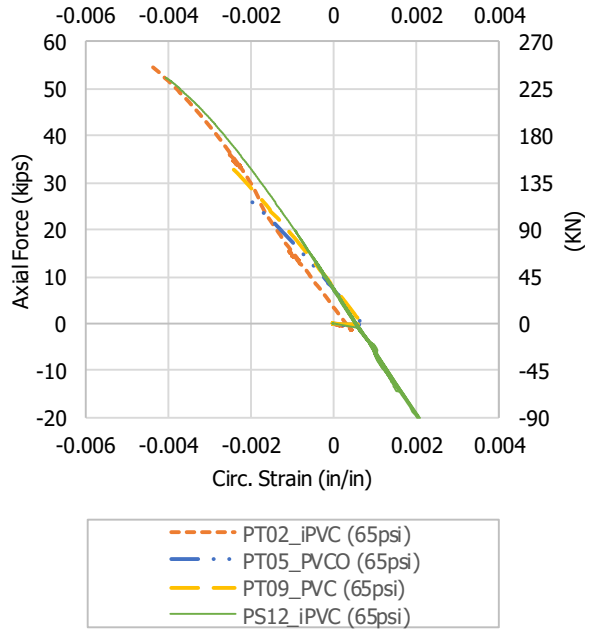


Figure 5.11. Tension Test Comparison for Axial Force vs Circ. Strain.



## 6. Summary and Conclusions

This study assesses the performance of thermoplastic pipe under external loading conditions associated with earthquakes and other sources of significant ground deformation. Axial tests on three types of pipe material with the same coupling were performed. Tests included four monotonic axial tension, one monotonic axial compression, and one axial cyclic test which imposed increasingly larger cycles of tensile and compressive loading prior to a monotonic axial pull to failure.

Table 6.1 provides a summary of the tests performed and key results. The three axial tests performed on iPVC pipe with RCT fitting achieved similar levels of axial force [52.3–55.3 kips (233-246 kN)] with only a 5% reduction in strength following cycles of tension/compression reaching an amplitude of 20 kips (88.9 kN), or approximately 36% of the ultimate joint strength. Joint opening at failure for all three tests were also reasonably consistent, 0.82-0.93 in. (21-24mm). The maximum axial tension strain recorded for the cyclic test (PS12) was 1.6%.

A single tension test was performed for each the PVC (C900, PC235) and PVCO (C909, PC305) materials with RCT joint. The PVC achieved a maximum axial force 17% larger than PVCO while the PVCO achieved a 15% greater axial strain and 32% greater joint opening at failure. These preliminary results suggest the PVCO (PC305) pipe-coupling systems would be capable of accommodating ~18% greater axial deformation over a standard 20-ft lay length than the PVC (PC235), and would therefore see a similar improvement in response to earthquake induced ground movement parallel to the pipe axis.

Table 6.1. Summary of Test Results

Test ID	Pipe-Coupling	Pipe PC (psi)	Internal Pressure @ Failure		Max. Actuator Force		Max. Axial Strain (%)	Act. Disp. at Failure		Joint Opening	
			psi	(kPa)	kips	(kN)		in.	(mm)	in.	(mm)
PT01	iPVC-RCT	305	0-5	(48)	55.3	(246)	NA	3.82	(97)	0.89	(23)
PT02	iPVC-RCT	305	60	(414)	55.3	(246)	NA	4.06	(103)	0.93	(24)
PT05	PVCO-RCT	305	63	(448)	28	(125)	1.17	2.96	(75)	0.70	(18)
PT09	PVC-RCT	235	65	(448)	33	(147)	1.02	2.47	(63)	0.53	(14)
PC06	PVCO-RCT	235	63	(434)	-16.2	(-72)	-2.0	-7.06	(-179)	-2.2	(-56)
PS12	iPVC-RCT	305	65	(448)	52.4	(233)	1.6	3.66	(93)	0.82	(21)



The results demonstrate the available axial capacity of the pipe coupling connection. These values can be used in assessing a system's expected performance to earthquake-induced ground deformation. Although some joint opening develops in response to axial loading, the coupling style would be considered a "restrained joint", as opposed to a hybrid segmented joint that allows significant joint opening, typically on the order of 1% of the pipe length. A restrained joint system, such as each of these tested, has superior capacity to resist ground deformation compared to un-restrained, push-on joint style connections.

While this testing program provides valuable results for assessing earthquake performance, additional assessment is recommended. Not all pressure classes and loading regimes were investigated for each joint type. Most tests were performed at a representative operating pressure, and variations may be possible based on internal pressure, specifically for thinner walled materials. Repeat tests, to identify variability in the experimental results, would be highly valuable for incorporation into seismic design assessments.



## Acknowledgements

The authors wish to recognize the excellent effort of University of Colorado students and staff that made these experiments successful. Namely, the contributions of graduate students David Kyle Anderson and Hailey-Rae Rose, and undergraduates David Balcells and Aldrich Valerian are gratefully acknowledged. Great thanks are extended to CIEST staff members Brice Lucero, Kent Polkinghorne, and John Hindman for their constant support and expertise.

Appreciation is extended to East Bay Municipal Utility District for technical and financial support for this study, especially colleagues David Katzev & Timothy Harris. The authors also thank the following industry representatives for providing restraints, couplings, and pipe specimens: EBAA Iron, Inc., JM Eagle, and PPI Pyungwha Co., Ltd.

## References

- Applied Technology Council. (2007). *FEMA 461: Interim Testing Protocols for Determining the Seismic Performance Characteristics of Structural and Nonstructural Components*. Redwood, CA: FEMA.
- AWWA. (2007). *AWWA C900-07 Polyvinyl Chloride (PVC) Pressure Pipe and Fabricated Fittings, 4 In. Through 12 In. (100 mm Through 300 mm), for Water Transmission and Distribution*. <https://doi.org/http://dx.doi.org/10.12999/AWWA.C900.07>
- AWWA. (2016). *AWWA C909-16 Molecularly Oriented Polyvinyl Chloride (PVCO) Pressure Pipe, 4 In. (100 mm) and Larger*. American Water Works Association (AWWA).
- Price, D., Berger, B. A., O'Rourke, T. D., Stewart, H. E., Wham, B. P., & Pariya-Ekkasut, C. (2018). *Performance Evaluation of iPVC Pipe under Earthquake-Induced Ground Deformation*. Ithaca, NY: Cornell University. Retrieved from <https://lifelines.cee.cornell.edu/projects/>
- Wham, B. P., Berger, B. A., Pariya-Ekkasut, C., O'Rourke, T. D., Stewart, H. E., Bond, T. K., & Argyrou, C. (2018). Achieving Resilient Water Networks – Experimental Performance Evaluation. In *Eleventh U.S. National Conference on Earthquake Engineering* (p. 11). Los Angeles, CA.
- Wham, B.P., Argyrou, C., O'Rourke, T.D., Stewart, H.E., Bond, T.K. (2017) PVCO Pipeline Performance Under Large Ground Deformation. *ASME Journal of Pressure Vessel Technology*. Vol.139(1). [10.1115/1.4033939](https://doi.org/10.1115/1.4033939)
- Wham, B.P., Berger, B.A., O'Rourke, T.D., Pariya-Ekkasut, C., Stewart, H. (2017). *Performance Evaluation of Bionax SR PVCO Pipeline with Extended Bell Joints under Earthquake-Induced Ground Deformation*, Technical Report. Ithaca, NY: Cornell University.



## Appendix A: Pressurization Sequence

The following section outlines the initial pressurization sequences performed prior to each of the axial tests. Several pressurizations were conducted prior to testing for several different reasons, including checking for initial leakage of the specimen, checking strain gage application and accuracy, and gaining better understanding of the specimen behavior under pressure. PS12 was used for sample data throughout this section.

iPVC pipe with an RCT coupling at the center joint was used for this study. The pipe was unrestrained axially to ensure true strain behavior under pressure. The specimen was filled with water and pressurized to ~65 psi (~450 kPa) three times per trial, shown in Figure 6.1. Strain data was recorded and compared to theoretical calculations, per Figure 6.2. The maximum circumferential strain recorded from the gages was 0.00059 in/in (0.059%) and the maximum axial strain recorded was 0.00012 in/in (0.012%).

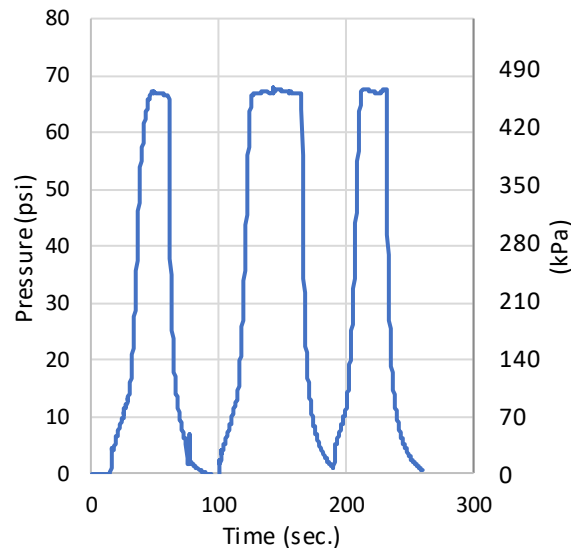


Figure 6.1. PS12 pressurization sequence, pressure vs time

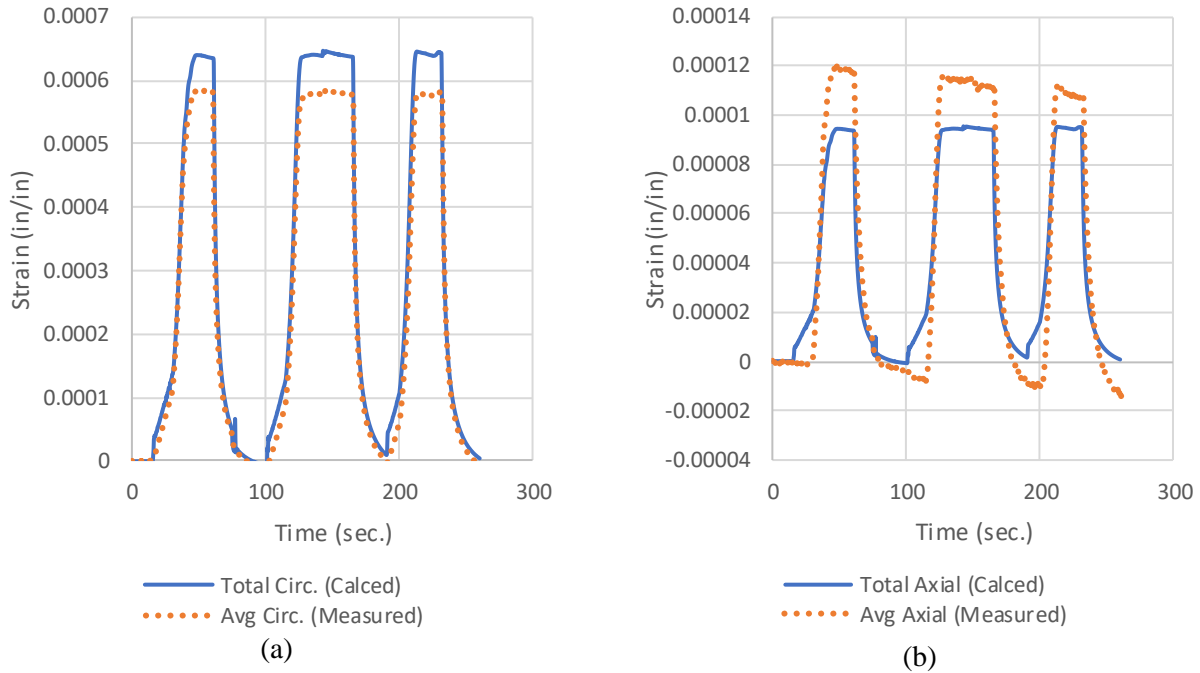


Figure 6.2. Circumferential (a) and Axial (b) strain vs time

Using the pressure recorded during the pressurization sequence, theoretical values for stress and strain were attained. The specimen was idealized as a thick-wall member; therefore, Equations 1 and 2 were used to solve for the circumferential and axial stress, respectively.

$$\sigma_{\theta} = \left[ \frac{2P_i r_i^2}{r_o^2 - r_i^2} \right] \quad \text{Eq. 1}$$

$$\sigma_z = \left[ \frac{P_i r_i^2}{r_o^2 - r_i^2} \right] \quad \text{Eq. 2}$$

$P_i$  is the internal pressure recorded during pressurization, and  $r_o$  and  $r_i$  are the outer radius and inner radius of the specimen, respectively. Once the stress was calculated, Hooke's law was applied to find strains associated with each stress, per Equation 3.

$$\varepsilon_i = \frac{\sigma_i}{E} \quad \text{Eq. 3}$$



450.3 ksi (XXX) was used as the Modulus of Elasticity (E) for the specimen, per Price et al., (2018). Equations 4 and 5 are used to find the total strain in each direction, taking into account Poisson's effect. A Poisson's ratio of 0.38 was used (Price et al., 2018).

$$\varepsilon_{\theta,T} = \varepsilon_{\theta} - \nu\varepsilon_z \quad \text{Eq.4}$$

$$\varepsilon_{z,T} = \varepsilon_z - \nu\varepsilon_{\theta} \quad \text{Eq.5}$$

The maximum theoretical circumferential strain was found to be 0.00065 in/in (0.065%) which was 8% more than the recorded value. The maximum theoretical axial strain was found to be 0.000096 in/in (0.0096%) which was 20% less than the recorded value. Considering the small scale of pressure applied to the specimen, the differences in strain can be a result of minor imperfections within the system. These results indicate that the strain gages used for testing record accurate data. This process was completed several times per test to ensure that the strain gages were installed properly.